High Frequency Permeability Measurements and Modeling of Magnetic Powder Cores Under DC Bias

Arne Schröder, *Member, IEEE*, Alexandru Savca, and Dierk Bormann

***Abstract*—Powder cores are attractive magnetic components for high-current applications due to their high saturation flux densities, combined with good high-frequency performance and relatively low losses. Although considered in many applications, only little information about their high-frequency properties under dc current bias exists. Therefore, this work describes a novel measurement methodology to determine the complex permeability of magnetic powder cores under superimposed dc bias. A comparison against alternative approaches reveals the advantages of the proposed methodology with respect to maximum frequency and bias current. Different types of powder cores are characterized at frequencies between 10 kHz and 100 MHz and superimposed currents up to 2.5 kA. Moreover, a simple phenomenological model is outlined that captures the permeability spectrum under dc bias. The model can conveniently be translated into equivalent circuits for use in system-level simulations.**

***Index Terms*—Electromagnetic compatibility, electromagnetic modeling, equivalent circuits, impedance measurement, permeability measurement, soft magnetic materials.**

I. Introduction

Passive magnetic components play a vital role in power electronic systems. Their optimization is indispensable to maximize the efficiency and to reduce both volume and cost of power electronic converters. Various classes of magnetic core materials exist, including for example laminated silicon steel, nanocrystalline alloys, ferrites, and powder cores. The choice of core material depends on the component type and its specific application [1]. For instance, the cores of common mode chokes with comparatively low net currents for use in electromagnetic interference (EMI) filters are usually made of low-loss ferrite or nanocrystalline material [2]. On the other hand, for applications involving high currents and associated high magnetic fluxes, powder core materials are often considered [1], [3], [4]. These are made of iron or alloy powder particles and exhibit distributed air gaps, providing high saturation flux density, low loss, competitive cost, and low hysteresis [5]. Soft saturation, elimination of fringing fields, and high Curie temperatures are advantages over gapped ferrites or nanocrystalline cores [4]. Furthermore, powder cores are considered to be promising candidates for high frequency (HF) converters [6]. In the field of electromagnetic compatibility (EMC), powder cores are applied for example in differential mode (DM) filters [7], [8].

For HF modeling and design of magnetic components, the availability of high-fidelity permeability data is crucial. This is especially true for components like single-turn inductors, e.g., [9], which do not suffer from parasitic effects, such as turn-to-turn capacitances, at high frequencies. Besides that, HF permeability data are required for fundamental research on magnetic materials. The HF complex permeability of magnetic materials is typically retrieved from complex impedance measurements on toroidal cores with multiple conductor turns, using LCR meters, impedance analyzers, or vector network analyzers [4], [10], [11]. To avoid inaccuracies caused by leakage flux of windings (which is more pronounced for low-permeability materials) or by stray capacitances of windings, one-port coaxial sample holders are usually employed [12], [13], [14], [15], [16], [17]. The maximum frequency for these setups is determined by the cavity resonance of the sample holder. Characterization up to several GHz is possible [13]. At even higher frequencies, the Nicolson-Ross-Weir method is typically applied, which deduces material properties from reflection and transmission measurements of material samples embedded in transmission lines [18], [19], [20].

The HF noise current on powder-core inductors is often much smaller than the fundamental frequency or dc current carried by the inductor. Accordingly, this HF noise effectively sees the differential (or "incremental") permeability of the material, which depends, in a nonlinear way, on a superimposed low-frequency or dc bias. Therefore, it is important to characterize the small-signal complex permeability as a function of a superimposed dc bias field.

A multiple-coil setup in which the dc current source is decoupled from the HF measurements via a decoupling network was used in [4]. A coaxial sample holder in conjunction with a bias-T decoupling network for bias currents up to 500 mA was employed in [21]. An impedance measurement setup with bias currents up to 200 A was presented in [22]. While the aforementioned setups rely on a galvanic contact between device under test and dc source, [23], [24] utilized a dc biasing via a secondary winding. A coaxial sample holder with bias field provided by a large external magnetic dipole magnet was employed in [25]. A cavity with parallel dc bias field was proposed in [26] and later built and used in [27]. General contactless

Manuscript received 3 April 2024; revised 14 June 2024; accepted 10 July 2024. Date of publication 18 July 2024; date of current version 7 October 2024. Recommended for publication by Associate Editor M. Shen. *(Corresponding author: Arne Schröder.)*

Arne Schröder and Alexandru Savca are with the Hitachi Energy Research, Segelhofstrasse 1A, 5405 Baden-Dättwil, Switzerland (e-mail: arne.schroeder@hitachienergy.com).

Dierk Bormann is with the Hitachi Energy Research, Västerås SE-722 26, Sweden (e-mail: dierk.bormann@hitachienergy.com).

Color versions of one or more figures in this article are available at https://doi.org/10.1109/TPEL.2024.3430200.

Digital Object Identifier 10.1109/TPEL.2024.3430200

impedance measurements of dc biased systems are subject to research [28], [29].

For fast and efficient designing of power converter systems and associated magnetic components, compact models of magnetic materials are required. Typically, equivalent circuits are used for the phenomenological modeling of magnetic properties. For example, Foster-type networks derived from measurements have been employed to describe the complex impedance of dc-biased nanocrystalline cores [23]. Cauer-type HF models combined with hysteresis and saturation models for nanocrystalline cores and ferrite cores were developed in [30] and later extended to account for dimensional resonance effects [31]. Higher-order Debye models with several discrete relaxation times were used in [32]. The complex permeabilities of magnetic powder materials were described in [33] by general Debye relaxation processes with continuous relaxation-time distributions.

While many works are devoted to investigation of losses in powder cores under dc bias (see, e.g., [34] and [35]), high frequency complex permeability of powder cores under superimposed dc bias has, to the best of our knowledge, not been studied yet. Therefore, this article aims at experimental characterization and modeling of the permeability of powder cores under dc bias for frequencies up to at least 100 MHz.

The rest of this article is organized as follows. Section II introduces a novel measurement setup for permeability characterization under dc bias. Section III assesses the proposed measurement setup and benchmarks it against alternative ones. Experimental characterization of two particular powder materials is described in Section IV, and a simple phenomenological model for the permeability under dc bias is outlined in Section V. Finally, Section VI concludes this article.

II. Measurement Setups

This section introduces a measurement setup for determining the complex permeability of toroidal magnetic powder cores under dc bias. Furthermore, three benchmark setups are described. We consider the complex relative permeability μ_r as function of angular frequency ω and superimposed dc current I_dc

$$\mu_\mathrm{r}(\omega, I_\mathrm{dc}) = \mu_\mathrm{r}'(\omega, I_\mathrm{dc}) - \mathrm{j}\,\mu_\mathrm{r}''(\omega, I_\mathrm{dc})\,. \tag{1}$$

In this work, core permeabilites are extracted from impedance measurements with a vector network analyzer (VNA). The dc bias current is provided by an external current source. A major challenge with this approach is to suppress the coupling between HF circuit and dc circuit. For this reason, some prior works used decoupling concepts with two identical powder cores (e.g., [23]). The setups outlined in the following sections employ a similar approach.

A. Decoupling of HF and DC Circuits

In all four setups to be described, an (ideally) perfect decoupling of the HF measuring circuit from the dc driving circuit is achieved using the same basic concept [23], illustrated in Fig. 2. The two circuits are galvanically isolated, and each of them uses a series-connected pair of identical windings around two (ideally) identical cores. The connections between windings are made in such a way that one of these pairs drives (ideally) equal parallel fluxes in the two cores ("series connection"), while the other drives *anti*parallel fluxes ("*anti*series connection"). In the proposed setup as well as in benchmark setups 1 and 2, the HF windings are antiseries connected in this sense, while in benchmark setup 3, the dc windings are antiseries connected. The decoupling effect is the same for all four variants of the concept (at least at low enough frequencies such that parasitic capacitances are negligible), and their main difference is the number of turns in the HF and dc windings, as described in the following.

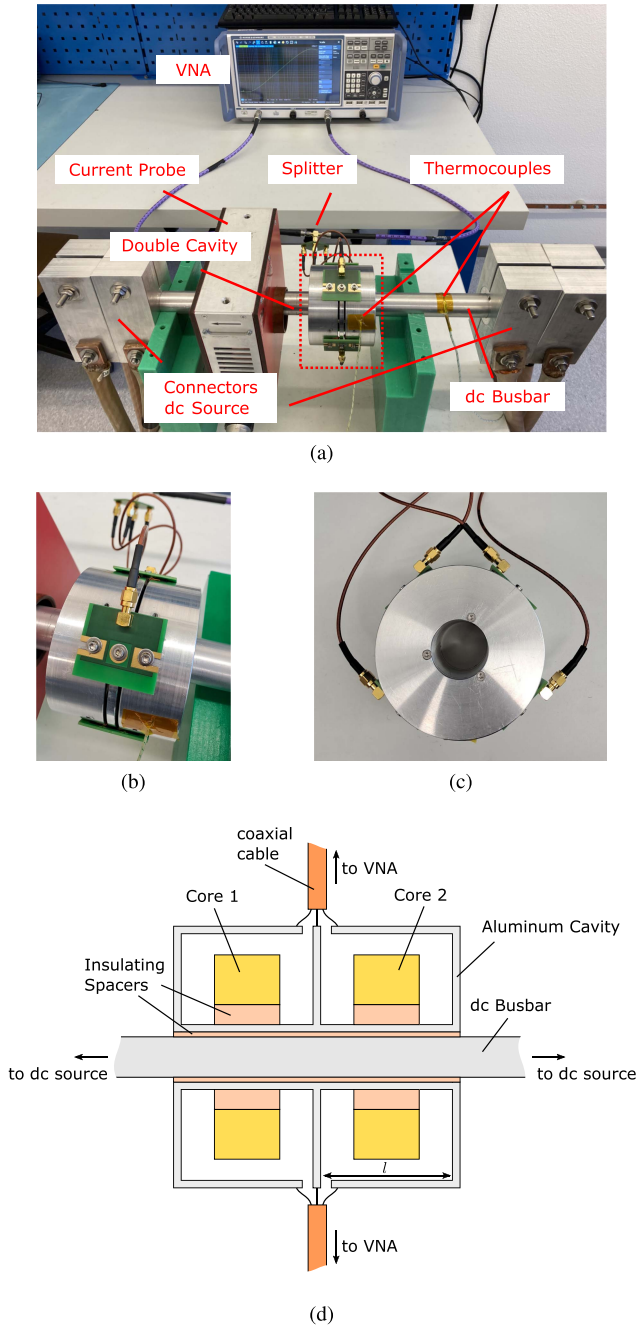

Fig. 1. Illustration of proposed double-cavity measurement setup to determine the complex impedance of magnetic powder cores under dc bias. (a) Photograph of setup in laboratory with (b) close-up view of the double cavity including SMA connection network and (c) connection points. (d) Cross section of double cavity. Each cavity includes one core.

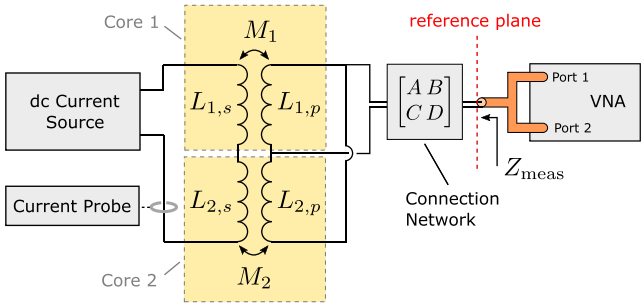

Fig. 2. Equivalent circuit of the setup 1, setup 2, and proposed setup.

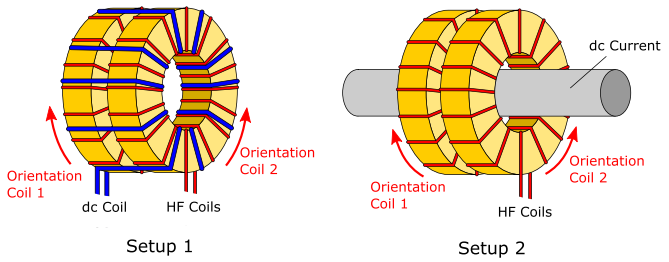

Fig. 3. Illustration of measurement setup 1 (left) and setup 2 (right) used to extract the complex permeability from toroidal cores with superimposed dc bias. The fluxes of the HF windings are oriented opposite to each other, to decouple the dc source from HF impedance measurements.

B. Proposed Setup - Double Cavity

The goal was to develop a measurement setup that can accurately determine permeability spectra of powder cores up to several tens of MHz under dc bias currents of more than 2 kA. To achieve a good high frequency performance, coils need to be avoided, as turn-to-turn capacitances cause coil resonances and deteriorate the high frequency accuracy. A single turn winding, as used in [23], [24], and [36], can be applied to avoid such coil resonances. However, stray fluxes diminish the accuracy when considering low-permeability cores such as powder cores. Therefore, the proposed setup is based on a shorted coaxial line [12], which minimizes stray fluxes and has a high upper frequency limit. The proposed setup consists of a double coaxial cavity which is arranged around a dc busbar with circular cross section, as illustrated in Fig. 1. Each cavity forms a shorted coaxial line and contains at least one toroidal core. The cores in both cavities are identical, consisting of the same material and having same dimensions, and are concentrically aligned by insulating spacers. A dc current source drives the current I_{dc} through the busbar and induces bias H-fields in the cores. Using nongalvanically connected dc sources avoids the usage of a decoupling inductor in the dc path [4], which would add a residual impedance to the HF path and potentially diminishes the measurement accuracy. The current is monitored by a flux-compensating current probe. In contrast to coaxial cavities for measurements without dc bias (like our reference setup discussed further below), the HF connection for the VNA cannot be placed centrally on the cylinder axis in this setup, since the dc conductor runs along this axis. To minimize stray magnetic fluxes caused by noncentered connection points, the double cavity is connected to the VNA on four equidistant points along its outer circumference via a connection network consisting of an SMA splitter with four legs.

An equivalent circuit of the setup is depicted in Fig. 2. Each cavity is coupled to the dc path by a certain mutual inductance M_i. The cavities are connected in series on the dc side and in antiparallel on the HF side. For identical cores $M_1 = M_2$, so that ideally there is no coupling between the dc and HF circuits. Thus, the measured impedance Z_{meas} is unaffected by the dc source impedance.

If the cavity length l is small compared to the electromagnetic wavelength in vacuum and attenuation is small ($\gamma l \ll 1$, with γ being the propagation constant in the cavity), the impedance of each cavity can be approximated as

$$Z_{\text{cav}} = Z_0 \tanh(\gamma l) \approx R_{\text{cav}} + \mathrm{j}\omega L_{\text{cav}}. \tag{2}$$

Here, Z_0 is the wave impedance of the vacuum, R_{cav} is the resistance, and L_{cav} is the inductance of each coaxial cavity. At high frequencies, cavity resonances occur and (2) does not hold. The first resonance of the considered cavity with $l = 30\,\text{mm}$ theoretically lies at 2.5 GHz. Extracting the permeability of magnetic cores with cavities is a well-established approach, see [12] for details, in which two different measurements are conducted: one with empty cavities, resulting in $Z_{\text{meas}}^{\text{empty}}$, and one with both cavities containing identical cores, resulting in $Z_{\text{meas}}^{\text{cores}}$. If (2) holds, the core permeability is determined by [12]

$$\mu_{\text{r}} = a \left[(Z_{\text{meas}}^{\text{cores}} - Z_{\text{meas}}^{\text{empty}}) \frac{l_{\text{e}}}{\mathrm{j}\omega\mu_0 A_{\text{e}}} + 1 \right], \tag{3}$$

where l_{e} is the effective magnetic length of the cores and A_{e} denotes the effective core cross section, e.g., [37]. As the cavity itself adds a certain inductance, the impedance of the empty cavity needs to be extracted to obtain the impedance of the core under test. In our case with two parallel cavities, a factor of $a = 2$ needs to be introduced to obtain the correct inductance.

A major advantage of this setup is the rotationally symmetric distribution within the cores of both dc and HF magnetic fields, which minimizes measurement inaccuracies due to stray flux. Furthermore, its upper limit frequency is determined by the cavity length only and not affected by any windings.

C. Benchmark Setups

Three benchmark setups to determine the complex permeability (1) with superimposed dc bias are outlined next.

1) Setup 1 and Setup 2 - Multiple HF Turns: Two setups with multiple HF turns are illustrated in Fig. 3. Both setups consist of two toroidal cores, each equipped with a HF winding of N turns. In addition, setup 1 uses a single dc bias winding with M turns encompassing both cores, while setup 2 uses a single busbar for biasing. To reach the same dc flux as in setup 1, the current in setup 2 needs to be M times higher than the current in setup 1. The HF windings are connected to a VNA. In both setups, the HF coils are connected in antiparallel, such that their fluxes have opposite orientation. Thereby, a decoupling of the HF circuit from the dc source is achieved, such that the HF impedance of the dc source only has a negligible effect on the impedance

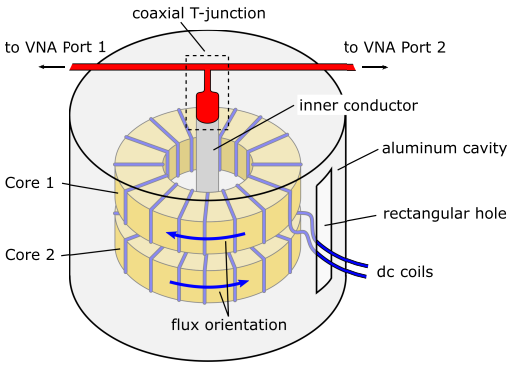

Fig. 4. Illustration of measurement setup 3. Two cores reside in a shorted coaxial cavity which is connected to the ports of a VNA via a T-junction. Both cores are biased by dc coils, with opposing flux orientation.

measurements, similarly to the proposed setup (Fig. 1). The complex permeability is extracted from the measured impedance using the equation

$$\mu_\mathrm{r} = Z_\mathrm{DUT} \frac{l_\mathrm{e}}{\mathrm{j}\omega\mu_0 A_\mathrm{e} N^2}, \tag{4}$$

where the core impedance Z_DUT is obtained from the measured impedance Z_meas by

$$Z_\mathrm{DUT} = 2(Z_\mathrm{meas} - R_\mathrm{HF}). \tag{5}$$

Here, the HF-coil resistance R_HF needs to be subtracted to obtain the correct μ_r'', and a factor 2 is introduced since the HF windings of the two cores are connected in parallel.

2) Setup 3 - Multiple DC Turns, Single HF Turn: Setup 3 is based on a shorted coaxial cavity, which encompasses two stacked cores, as depicted in Fig. 4. Each core is biased by an individual dc coil. The dc coils are connected in antiseries now, to decouple the HF circuit from the dc source, as before. The connection wires are guided from the dc source to the coils through a rectangular hole in the cavity.

3) Setup to Obtain Reference Values: To obtain reference values for unbiased cores, we have conducted measurements using a shorted coaxial aluminium cavity, a well-established setup [12], with an inner diameter of 80 mm and an inner height of 25 mm. As there are no coils involved in this setup and the lowest cavity resonance lies at around 3 GHz, the obtained results are considered as reference values.

III. Assessment of Proposed Measurement Setup

We conducted assessment measurements for frequencies between 9 kHz and 110 MHz. Two different powder cores as specified by Table I were used: Carbonyl iron powder *Mix 26* from *Micrometals* [38] and *Mega Flux* (silicon iron powder) from *Chang Sung Corporation* [37]. These materials had been chosen for their different properties: for instance, *Mega Flux* saturates at higher magnetic fields than *Mix 26*, and its high frequency properties are superior to those of *Mix 26*.

Measurements were conducted with a *Rohde and Schwarz ZNB 8* VNA. We performed two-port shunt-through measurements [35] to obtain the impedances of the cores under test. Thanks to the high dynamic range of the VNA, very low impedances can be extracted by this procedure. In our case, the smallest measured impedances were below 2.5 mΩ. Nevertheless, due to low DUT impedances at the low frequency end, measurements are affected by the VNA's noise floor. To improve the signal-to-noise ratio (SNR) in the low frequency region, the entire frequency band was split into four channels with individual measurement bandwidths. For instance, the first channel measured from 9 to 20 kHz with 1 Hz bandwidth, while the fourth channel measured from 1 to 110 MHz with 100 Hz bandwidth. This channel split improves the SNR considerably, while keeping the acquisition time low. To further improve the SNR, an elevated output power of 10 dBm was applied.

TABLE I
Comparison of Measurement Setups for Characterization of Complex Permeability of Magnetic Powder Cores

Material	*Mix 26*	*Mega flux*
Core number	T300-26	CK77860
Manufacturer	Micrometals	CSC
Initial μ_r	75	60
Path length l_e	198 mm	200 mm
Cross section A_e	338 mm^2	277 mm^2
A_L	160 nH	85 nH
B_sat	1.38 T	1.6 T

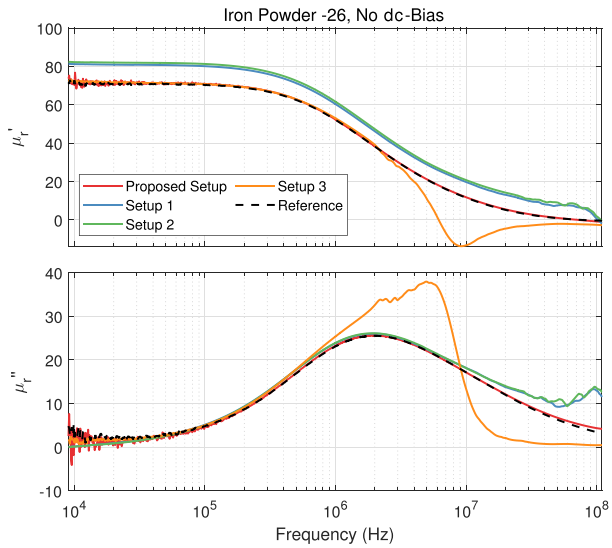

Fig. 5. Measured complex permeability of iron powder *Mix 26* using different setups. DC bias current is zero.

A. Comparison of Setups

A comparison of permeability spectra measured with the different setups, for *Mix 26* under zero dc bias current, is depicted in Fig. 5. The permeability of this material shows a typical relaxation type behavior [33]. The permeability retrieved by the proposed measurement setup agrees very well with the reference results that were obtained with a single cavity described in Section II-C3. A slightly higher real part is observed in the entire frequency range, see discussion in Section III-C, and slight deviations are observed at the high frequency end, see discussion in Section III-B. Both setups 1 and 2 with ten HF turns result in a higher real part of the permeability due to stray inductances. The

TABLE II
MEASUREMENT SETUP COMPARISON FOR CHARACTERIZATION OF COMPLEX PERMEABILITY SPECTRA OF MAGNETIC POWDER CORES UNDER DC BIAS

	Proposed setup	**Setup 1**	**Setup 2**	**Setup 3**
Description	Double HF cavity, single dc busbar (no coils)	Cores with both dc and HF coils	Cores with HF coils, single dc busbar	Cores with dc coils, single HF cavity
# Turns HF coils **# Turns dc bias coils** **Max. frequency**	1 1 >100 MHz	10 25 10 MHz	10 1 10 MHz	1 25 1 MHz
Advantages	• High bias fields • Large frequency range 9 kHz–100 MHz	• *Low*-current dc source sufficient	• Simple Setup • High bias fields	• *Low*-current dc source sufficient
Disadvantages	• High-current dc source required	• Max. dc current limited by wire heating • High effort for preparation of bias windings • Calibration for stray fields required • Max. freq. < 10 MHz	• High-current dc source required • Calibration for stray fields required • Max. freq. < 10 MHz	• High effort for preparation of bias windings • Max. freq.< 1 MHz

imaginary part agrees very well with the reference up to 10 MHz; above that frequency, a slight deviation is noticeable. Setup 3 exhibits very good agreement with the reference results up to 1 MHz, while above 1 MHz the accuracy is strongly diminished by the turn-to-turn capacitances of the bias coils. Since only the proposed setup exhibits a good performance in the entire frequency range, the following investigations focus on the proposed setup. Table II summarizes pros and cons of all compared setups. The main advantages of the proposed setup are its wide frequency range and the high achievable bias fields. The wide frequency range is obtained as there are no coils involved, neither on the HF side nor on the dc side (in contrast to the benchmark setups). Accordingly, potential resonances caused by turn-to-turn capacitances of coils are circumvented and their negative impact on measurement is avoided. In addition, this setup does not suffer from effects of stray fluxes like those occurring in setups 1 and 2. The main disadvantage is the required high current rating of the dc source and associated cables and connectors, which are more expensive and bulky than those used in setup 1 and setup 3.

B. De-Embedding of Connection Network

The VNA was calibrated at the reference plane behind the SMA T-junction, as shown in Fig. 2. The T-junction was connected with the double cavity by a connection network consisting of a four way SMA splitter and four SMA cables. At low frequencies, the network has both resistive and inductive behavior, and its contribution to the permeability is canceled out when subtracting the measured empty cavity impedance in (3). At higher frequencies, the network needs to be de-embedded.

In this work, we represent the connection network by ABCD matrices [39]. Using this, the actual impedance of interest Z_{DUT} can be obtained from the measured impedance Z_{meas} by

$$Z_{\mathrm{DUT}} = \frac{(Z_{\mathrm{O}} - Z_{\mathrm{L}})\,(Z_{\mathrm{meas}} - Z_{\mathrm{S}})}{(Z_{\mathrm{L}} - Z_{\mathrm{S}})\,(Z_{\mathrm{O}} - Z_{\mathrm{meas}})} 50\,\Omega\,. \tag{6}$$

Here, Z_{O} is the measured impedance with the connection network ends being open, Z_{S} is the measured impedance with the connection network ends being shorted, and Z_{L} is the measured impedance with the connection network ends being terminated with $50\,\Omega$. We have used dedicated open, short, and load PCB terminations with the same PCB design as the SMA to cavity interface. The open, short, and load terminations are illustrated in Fig. 6.

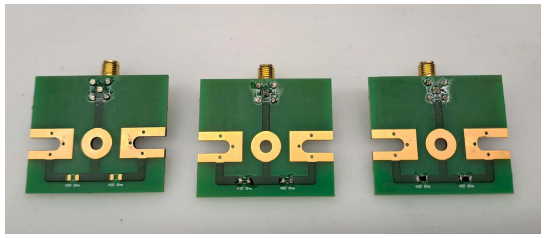

Fig. 6. Custom-made PCB calibration loads used for de-embedding. From left to right: Open, short, and load.

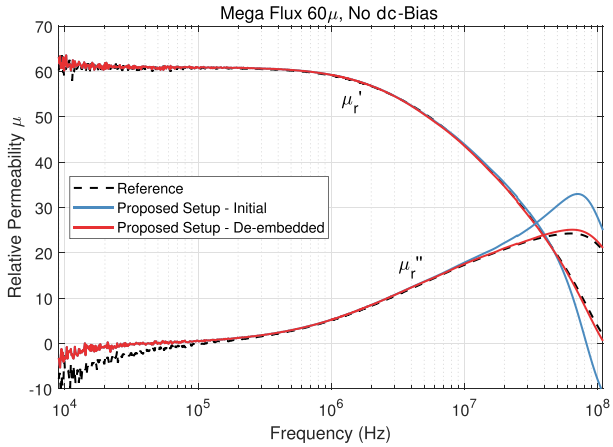

Fig. 7. Validation of de-embedding of connection network from proposed setup: Measured permeability of *Mega Flux* cores at zero dc bias obtained with proposed setup and single-cavity reference setup.

Fig. 7 compares the permeability of the *Mega Flux* cores obtained by the proposed setup, with and without de-embedding, with results from the reference setup. Without de-embedding, differences to the reference become visible above 10 MHz,

whereas a good agreement with the reference is obtained after de-embedding.

C. Error Discussion and Data Smoothing

We have observed that the two main contributors to measurement errors are as follows: 1) limited sensitivity of the VNA at low frequencies and 2) variation of the measured resistance between empty and loaded cavity measurements. A resistance variation ΔR can originate from variations of contact resistance or temperature during measurements. It affects the retrieved imaginary part of the permeability

$$\Delta\mu_{\mathrm{r}}'' = \Delta R \frac{2l_{\mathrm{e}}}{\omega\mu_0 A_{\mathrm{e}}}, \tag{7}$$

see (3). The error is inversely proportional to frequency and thus, most pronounced in the low frequency range. For the considered examples, a variation of 1 $\mathrm{m\Omega}$ results in $\Delta\mu_{\mathrm{r}}'' > 6$ at 10 kHz. Therefore, to obtain the actual μ_{r}'', we extract it instead from the measured μ_{r}' via the Kramers–Kronig relation [40]

$$\mu_{\mathrm{r}}''(\omega) = -\frac{2\omega}{\pi}\mathcal{P}\int_0^\infty \frac{\mu_{\mathrm{r}}'(\omega')}{\omega'^2 - \omega^2}\,\mathrm{d}\omega', \tag{8}$$

where $\mathcal{P}$ denotes the Cauchy principal value. For the numerical evaluation of (8), we smooth the measured μ_{r}' data using a sixth order polynomial fit and extrapolation towards a constant value at low frequency. At frequencies above 10 MHz, we use the measured μ_{r}'' instead of μ_{r}'' obtained from (8), to avoid artifacts arising from the finite upper frequency limit.

Besides the error sources mentioned above, we noticed a slight stray inductance due to the four-point HF connection, described in Section II-B, and the resulting nonuniform azimuthal H-field. We experimentally determined a value of around 1.4 nH and corrected the measured data accordingly.

Moreover, note that the bias H-field is not constant in radial direction with respect to the dc busbar. As a consequence, the core is biased nonuniformly and exhibits a spatial, nonuniform permeability distribution under dc bias. With the outlined measurement procedure, an averaged permeability for a certain core dimensions is extracted. We determined that the error introduced by this averaging is less than 1% compared with an infinitesimal thin toroid, for the materials and dimensions considered. Furthermore, we noted that manufacturing tolerances lead to noticeably different permeability spectra. For instance, the dissipation peak frequencies of ten *Mix 26* cores varied by more than 1 MHz. For this reason, we have selected two cores with similar permeability spectra for measurements with superimposed bias.

IV. Examples

The complex permeability under superimposed dc bias field of the two example materials shown in Table I was experimentally characterized with the proposed setup. We have used three parallel-connected Agilent 6680 A dc current sources to obtain a maximum bias current of 2.5 kA, resulting in a mean dc field of 157.8 Oe in the considered cores. Measurements were conducted sequentially at bias currents between 0 A and 2.5 kA with 250 A increments.

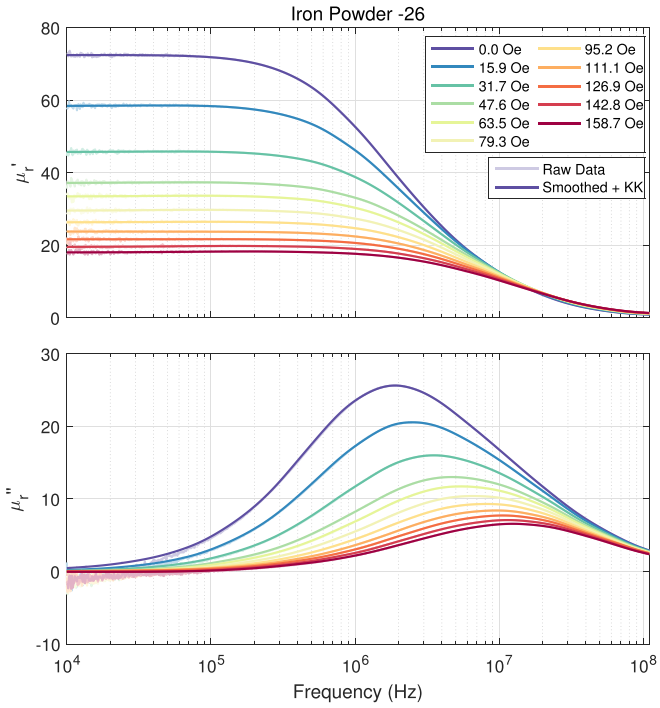

Fig. 8. Measured complex permeability of *Mix 26* for various dc bias fields. The measured raw data has been smoothed and the imaginary part up to 10 MHz extracted by Kramers–Kronig (KK) relation, see Section III-C.

Due to conduction losses, the measurement setup heated up, resulting in core temperature increases by max. 20 °C. Temperature effects on permeability were neglected, since the considered materials show less than 2% permeability variations within the measured temperature span, according to data sheets.

We noticed that the inductance of the empty test fixture between 9 and 100 kHz slightly decreased under a bias current. This effect is probably due to the fact that the aluminum alloy contains a small amount ($<0.5\%$) of magnetic iron which reduces the inner inductance of the test setup when saturating. Therefore, to evaluate (3), measurements of the empty test fixture were conducted separately for each bias current value.

Fig. 8 shows the measured complex permeability of *Mix 26* for various dc bias fields between 0.0 and 157.8 Oe. The permeability decreases with increased bias field due to partial saturation of powder core particles. Its real part drops with frequency and tends to zero at high frequencies. With increasing dc bias, the dissipation peak of the imaginary part is shifted towards higher frequencies.

Fig. 9 shows the measured complex permeability of *Mega Flux* for various dc bias fields between 0.0 and 157.8 Oe. A similar behavior as for the *Mix 26* is observed. However, the permeability decrease with dc bias is slower than for *Mix 26*, due to the lower initial permeability and higher saturation flux density of *Mega Flux*. Furthermore, the real part decline sets in at higher frequencies than for *Mix 26*. Accordingly, the dissipation peak in the imaginary part is located at higher frequencies. Furthermore, the dissipation peak has a different shape compared

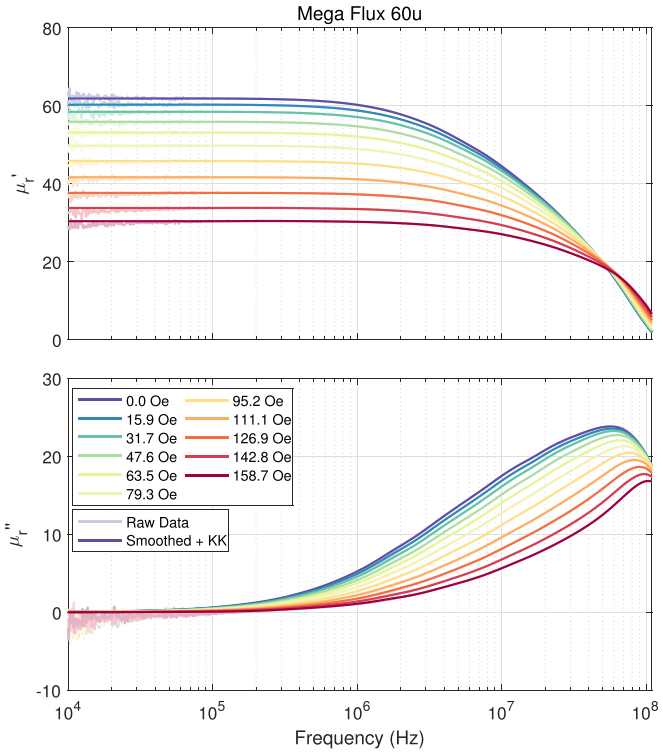

Fig. 9. Measured complex permeability of *Mega Flux* for various dc bias fields. The measured raw data has been smoothed and the imaginary part up to 10 MHz extracted by Kramers–Kronig (KK) relation, see Section III-C.

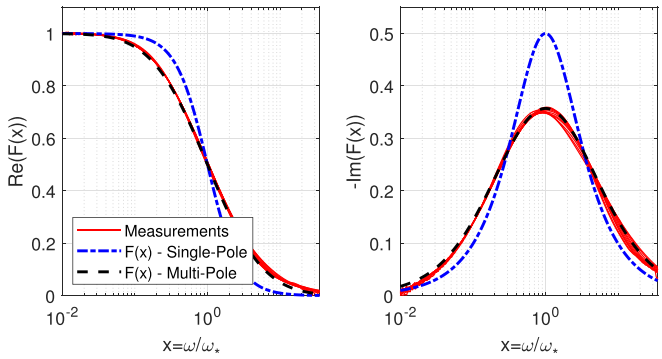

Fig. 10. Scaled experimental data (red) plotted together with discrete-sum approximation (13) of the scaling function with $n = 7$ terms (black dashed curve). The single-pole form (blue dotted curve) is shown for comparison. Considered material is *Mix 26*.

with the *Mix 26* and the real part exhibits a trend towards negative values. These differences are caused by dimensional resonances in the core [41].

V. Phenomenological Model

This section outlines a simple phenomenological model of the complex permeability $\mu_\mathrm{r}(\omega, I_\mathrm{dc})$ of powder core materials, capturing its dependence on both frequency and dc bias. We extend the higher-order Debye modeling approach [32] by combining it with a scaling assumption for the dc bias dependence, which leads to a simple phenomenological model with a small number of adjustable parameters. The model has a natural representation by a R-L Foster circuit with bias dependent circuit elements. Moreover, the model parameters have simple physical meanings and can directly be inferred from measurements.

A. Scaling With DC Bias

In our measurements, we have observed that the bias dependence of pure material characteristics, like those for *Mix 26* shown in Fig. 8, can be described as follows by a simple, approximate scaling law (note that this is not possible in more complex situations where resonance effects of the measuring setup become visible, like those for *Mega Flux* shown in Fig. 9).

As seen in Fig. 8 for the example of *Mix 26*, the static permeability $\mu_\mathrm{r}(0, I_\mathrm{dc})$ is a decreasing function of I_dc. Let $\omega_*(I_\mathrm{dc})$ denote the bias dependent frequency of the dissipation peak (i.e., the maximum of μ_r'' as a function of ω), which is an increasing function of I_dc. Assuming a proportionality $\omega_*(I_\mathrm{dc}) \propto \mu_\mathrm{r}(0, I_\mathrm{dc})^{-\beta}$ with some exponent $\beta > 0$, we can then, for any given I_dc, plot real and imaginary parts of the normalized permeability $\mu_\mathrm{r}(\omega, I_\mathrm{dc})/\mu_\mathrm{r}(0, I_\mathrm{dc})$ versus the scaled frequency $\omega/\omega_*(I_\mathrm{dc})$. Combining all plots for different I_dc and adjusting the value of β, one can obtain a quite good collapse onto a single curve (see Fig. 10, showing the same data as Fig. 8, but scaled with $\beta = 1.2$). This means that our data approximately obey a scaling law, characterized by the exponent β and a "universal" (for the given material) scaling function F that represents all collapsed curves in Fig. 10. The peak of $-\mathrm{Im}F(x)$ is located at $x = 1$. The scaling law may be written in the following way: for any ω and I_dc,

$$\frac{\mu_\mathrm{r}(\omega, I_\mathrm{dc})}{\mu_\mathrm{r}(0, I_\mathrm{dc})} = F\left(\frac{\omega}{\omega_*(I_\mathrm{dc})}\right) = F\big(C\omega\,\mu_\mathrm{r}(0, I_\mathrm{dc})^\beta\big), \qquad (9)$$

where the constant C can be determined for instance from the zero-bias ($I_\mathrm{dc} = 0$) data:

$$C^{-1} = \omega_*(0)\,\mu_\mathrm{r}(0,0)^\beta\,. \qquad (10)$$

The scaling function F can be approximated by a higher-order Debye function [32] describing relaxation times distributed in some range around ω_*^{-1}, i.e., by a rational function with some distribution of poles on the positive imaginary axis, with locations close to j. Note that a simple single-pole form $\left(F(x) = \frac{1}{1+\mathrm{j}x}\right)$ is insufficient, since its imaginary part has a peak height of $-\mathrm{Im}F(1) = 0.5$, instead of the value ≈ 0.35 implied by our measurements (Fig. 10). A distribution of pole locations over some interval is required to obtain a satisfactory fit of height and width of the peak. The end result for the scaling function $F(x)$ at real arguments x mainly depends on center position and width of this distribution but is rather insensitive to its detailed shape.

B. Debye Model for the Permeability Function

In practice, random quantities that are strictly positive (like, in our case, the relaxation rates in a Debye model) are often well

described by a log-normal distribution [42]. Here, we choose the relaxation rates to be log-normal distributed with mean zero and (dimensionless) variance σ^2, which we write in the following way:

$$F(x) = \frac{1}{\sqrt{2\pi\sigma^2}} \int_{-\infty}^{+\infty} \frac{\mathrm{e}^{-u^2/2\sigma^2}}{1+\mathrm{e}^u \mathrm{j}x}\,\mathrm{d}u\,. \tag{11}$$

In fact, the results for μ_r are rather insensitive to the detailed shape of this distribution, so other choices are equally possible. The choice (11) has the convenient property that its peak is always located exactly at $x = 1$ for any value of σ^2, since $-\mathrm{Im}F(x)$ is an even function of $\log x$. This nice property is preserved when the integral in (11) is replaced by a sum over discrete values u_i that are placed symmetrically around $u = 0$. For instance, we may use n equidistant values u_i between -2σ and 2σ:

$$u_i = 2\sigma \frac{2i-n-1}{n-1}\,. \tag{12}$$

The integral (11) is then replaced by a sum

$$F(x) = \sum_{i=1}^{n} \frac{\alpha_i}{1+\mathrm{e}^{u_i}\mathrm{j}x}, \tag{13}$$

with discrete weights α_i given by

$$\alpha_i = \frac{\mathrm{e}^{-u_i^2/2\sigma^2}}{\sum_{j=1}^{n} \mathrm{e}^{-s_j^2/2\sigma^2}}\,. \tag{14}$$

In Fig. 10, a scaling function F of the form (13) is plotted together with our scaled measurement results. Here, we have chosen $n = 9$ (further increasing n did not noticeably improve the agreement with the measurements). Note that the weights α_i are *not* independent fitting parameters here: the whole scaling function F only has a single adjustable parameter σ^2, whose value $\sigma^2 \approx 1.24$ is fixed by the requirement that the peak height of the imaginary part of F should match the measured value ≈ 0.35. This "one-parameter fit" is seen to result in good agreement over the whole argument range, the error being comparable to the deviations of our measurements from perfect scaling behavior. For comparison, also the (clearly unsatisfactory) single-pole form $F(x) = \frac{1}{1+\mathrm{j}x}$ is shown in Fig. 10.

Finally, substituting the argument of F in (9) back into (13), we obtain the following approximate expression for the complex permeability function:

$$\mu_\mathrm{r}(\omega, I_\mathrm{dc}) = \mu_\mathrm{r}(0, I_\mathrm{dc}) \sum_{i=1}^{n} \frac{\alpha_i}{1+\mathrm{j}\omega\,\tau_i(I_\mathrm{dc})}, \tag{15}$$

with weights α_i as defined in (14) and relaxation times

$$\tau_i(I_\mathrm{dc}) = \mathrm{e}^{u_i} C\,\mu_\mathrm{r}(0, I_\mathrm{dc})^\beta = \frac{\mathrm{e}^{u_i}}{\omega_*(0)} \left(\frac{\mu_\mathrm{r}(0, I_\mathrm{dc})}{\mu_\mathrm{r}(0,0)}\right)^\beta. \tag{16}$$

Thus, if scaling holds, then the dc-bias-dependent dynamic permeability of the powder core material is fully characterized by the bias dependence of the static permeability, along with only three additional empirical parameters, as follows.

1) The frequency $\omega_*(0)$ of the dissipation peak without bias.
2) The relative height of this dissipation peak [alternatively, the variance σ^2 of the log-normal distribution in (11)].
3) The dynamic scaling exponent β in (9).

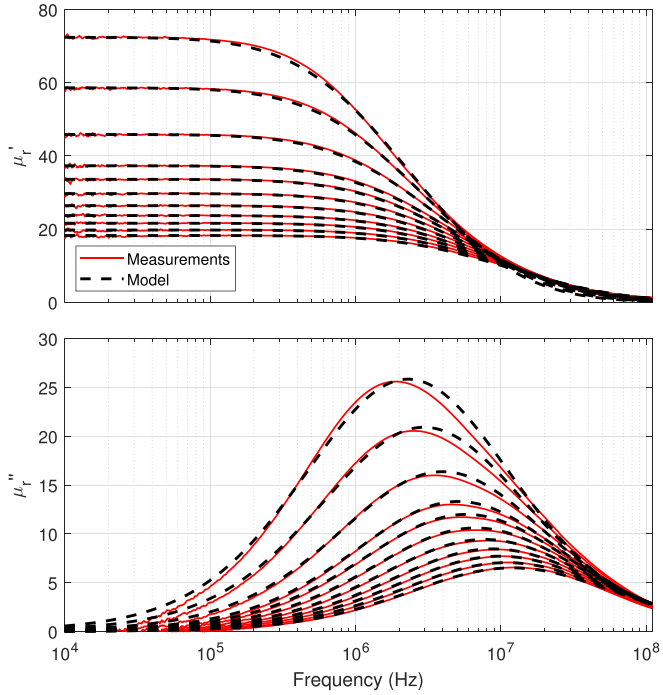

Fig. 11. Permeability spectra for various dc bias fields obtained by measurements and proposed permeability model. Considered material is *Mix 26*, see also Fig. 8.

Fig. 11 compares the measured permeability of *Mix 26* with the outlined model. A very good agreement is observed. Slight differences go back to the simplistic nature of the model.

C. Circuit Representation

We may use (15) to represent the impedance Z_DUT, which is related to μ_r by (4), as an electrical circuit. For instance, coded in the form of a SPICE netlist, it can then be incorporated in a variety of simulation environments that support this syntax. This is convenient for building HF models of electrical components containing powder cores and for their integration into system level simulations.

As an illustration, we consider the simple example defined in the previous section, with parameter values $n = 9$, $\sigma^2 = 1.24$, and $\omega_*(0)/2\pi = 2.3\times10^6$ Hz. From (13) to (16), we obtain

$$Z_\mathrm{DUT}(\omega, I_\mathrm{dc}) = \sum_{i=1}^{n} \left(\frac{1}{\mathrm{j}\omega\,L_i(I_\mathrm{dc})} + \frac{1}{R_i(I_\mathrm{dc})}\right)^{-1}, \tag{17}$$

with new definitions

$$L_i(I_\mathrm{dc}) = L_0 \alpha_i\,\mu_\mathrm{r}(0, I_\mathrm{dc})\,, \tag{18a}$$

$$R_i(I_\mathrm{dc}) = L_i(I_\mathrm{dc})/\tau_i(I_\mathrm{dc})\,, \tag{18b}$$

$$L_0 = \mu_0 \frac{A_\mathrm{e}}{l_\mathrm{e}}, \tag{18c}$$

where $\tau_i(I_\mathrm{dc})$ is defined by (16). Expression (17) for Z_DUT is just the frequency-dependent impedance of an R-L Foster circuit with bias-dependent inductances L_i and resistances R_i (Fig. 12), whose conversion into a SPICE netlist is straightforward. In

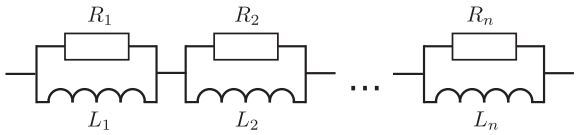

Fig. 12. Foster circuit with n L-R elements and modeling the bias-dependent impedance (17) of a magnetic powder core.

TABLE III
L-R CIRCUIT ELEMENT VALUES FOR THE FOSTER REPRESENTATION IN FIG. 12 OF MATERIAL *MIX 26* AT DIFFERENT BIAS CURRENTS AND BIAS H-FIELDS, RESPECTIVELY

I_{dc}	0	0.5	1	1.75	2.5	0	0.5	1	1.75	2.5
H_{dc}	0	31.7	63.5	111	159	0	31.8	63.5	111	159
$i \downarrow$	$\downarrow \frac{L_i(I_{\mathrm{dc}})}{L_0} \downarrow$					$\downarrow \frac{R_i(I_{\mathrm{dc}})}{L_0\,\omega_*(0)} \downarrow$				
1	0.01	0.01	0.00	0.00	0.00	0.00	0.00	0.00	0.00	0.00
2	0.32	0.20	0.15	0.11	0.08	0.01	0.01	0.01	0.01	0.01
3	3.91	2.48	1.81	1.28	0.99	0.42	0.46	0.49	0.53	0.56
4	17.5	11.1	8.13	5.73	4.42	5.75	6.30	6.71	7.19	7.58
5	28.9	18.3	13.4	9.45	7.28	28.9	31.6	33.7	36.1	38.0
6	17.5	11.1	8.13	5.73	4.42	53.4	58.5	62.2	66.7	70.3
7	3.91	2.48	1.81	1.28	0.99	36.3	39.7	42.3	45.3	47.8
8	0.32	0.20	0.15	0.11	0.08	9.06	9.93	10.6	11.3	11.9
9	0.01	0.01	0.00	0.00	0.00	0.83	0.91	0.97	1.04	1.10

Bias I_{dc} values are given in kA, corresponding H_{dc} values in Oersted.

Table III, values of the dimensionless parameter combinations $\frac{L_i(I_{\mathrm{dc}})}{L_0}$ and $\frac{R_i(I_{\mathrm{dc}})}{L_0\,\omega_*(0)}$, which characterize this specific model of *Mix 26*, are collected for a subset of the dc bias values that were used in Figs. 8 and 11.

Before implementation, the Foster circuit in Fig. 12 can of course be converted to an alternative circuit topology, like an equivalent Cauer circuit. However, since its present purpose is illustrative only, we are not concerned with optimizing the form of its practical implementation in any way.

VI. CONCLUSION

This article proposes a measurement setup for determining the high frequency, complex permeability of magnetic powder cores under dc bias. The proposed setup has been benchmarked against three alternative setups. The main advantage of the proposed setup compared to existing alternatives is its wide applicable frequency range of up to at least 100 MHz. For the first time, the high-frequency spectra of two different powder core materials are analyzed under dc bias. Moreover, a simple extension of a higher-order Debye modeling approach is outlined, combining it with a scaling form of the dc bias dependence. Our model has only three adjustable parameters, which moreover have clear physical meanings, and it can easily be represented by an R-L Foster circuit with bias dependent circuit elements. Due to its simplicity and the excellent fit, the proposed model can efficiently be applied in system-level EMC simulations, for designing, e.g., EMC filters.

In future works, the phenomenological model should be benchmarked against black-box models, such as those obtained by Vector Fitting. Furthermore, the phenomenological model should be extended to capture also dimensional resonance effects like those we observed in the *Mega Flux* cores.

ACKNOWLEDGMENT

The authors like to thank Christian Bottali and Domenic Burri and their team for manufacturing the measurement cavities used in this work, as well as their esteemed colleagues Ralph Burkart, Thomas Gradinger, Yunni Li, and Pritam Mukherjee for a critical reading of the manuscript and helpful suggestions.

REFERENCES

[1] M. S. Rylko, B. J. Lyons, J. G. Hayes, and M. G. Egan, "Revised magnetics performance factors and experimental comparison of high-flux materials for high-current DC–DC inductors," *IEEE Trans. Power Electron.*, vol. 26, no. 8, pp. 2112–2126, Aug. 2011.

[2] M. Kacki, M. S. Rylko, J. G. Hayes, and C. R. Sullivan, "Magnetic material selection for EMI filters," in *Proc. 2017 IEEE Energy Convers. Congr. Expo. (ECCE)*, 2017, pp. 2350–2356.

[3] Y. Liu, H. A. Mantooth, J. C. Balda, and C. Farnell, "A variable inductor based LCL filter for large-scale microgrid application," *IEEE Trans. Power Electron.*, vol. 33, no. 9, pp. 7338–7348, Sep. 2018.

[4] J. Imaoka, K. Okamoto, M. Shoyama, Y. Ishikura, M. Noah, and M. Yamamoto, "Modeling, magnetic design, simulation methods, and experimental evaluation of various powder cores used in power converters considering their dc superimposition characteristics," *IEEE Trans. Power Electron.*, vol. 34, no. 9, pp. 9033–9051, Sep. 2019.

[5] H. Shokrollahi and K. Janghorban, "Soft magnetic composite materials (SMCs)," *J. Mater. Process. Technol.*, vol. 189, no. 1, pp. 1–12, 2007.

[6] C. Jiang, X. Li, S. S. Ghosh, H. Zhao, Y. Shen, and T. Long, "Nanocrystalline powder cores for high-power high-frequency power electronics applications," *IEEE Trans. Power Electron.*, vol. 35, no. 10, pp. 10821–10830, Oct. 2020.

[7] M. L. Heldwein and J. W. Kolar, "Impact of EMC filters on the power density of modern three-phase PWM converters," *IEEE Trans. Power Electron.*, vol. 24, no. 6, pp. 1577–1588, Jun. 2009.

[8] D. O. Boillat, F. Krismer, and J. W. Kolar, "EMI filter volume minimization of a three-phase, three-level T-type PWM converter system," *IEEE Trans. Power Electron.*, vol. 32, no. 4, pp. 2473–2480, Apr. 2017.

[9] M. Szewczyk, W. Piasecki, M. Stosur, M. Florkowski, and U. Riechert, "Damping of VFTO in gas-insulated switchgear by a new coating material," *IEEE Trans. Power Del.*, vol. 31, no. 6, pp. 2553–2558, Dec. 2016.

[10] C. Cuellar, W. Tan, X. Margueron, A. Benabou, and N. Idir, "Measurement method of the complex magnetic permeability of ferrites in high frequency," in *Proc. 2012 IEEE Int. Instrum. Meas. Technol. Conf. Proc.*, 2012, pp. 63–68.

[11] R. Suárez, M. Tijero, R. Moreno, A. Arriola, and J. M. González, "3-D modeling and characterization of ferrite and nanocrystalline magnetic cores for EMI applications," in *Proc. 2023 IEEE Symp. Electromagn. Compat. Signal/Power Integrity (EMC SIPI)*, 2023, pp. 28–33.

[12] R. B. Goldfarb and H. E. Bussey, "Method for measuring complex permeability at radio frequencies," *Rev. Sci. Instruments*, vol. 58, no. 4, pp. 624–627, 1987.

[13] J. Shenhui and J. Quanxing, "An alternative method to determine the initial permeability of ferrite core using network analyzer," *IEEE Trans. Electromagn. Compat.*, vol. 47, no. 3, pp. 651–657, Aug. 2005.

[14] R. Huang and D. Zhang, "Using a single toroidal sample to determine the intrinsic complex permeability and permittivity of Mn–Zn ferrites," *IEEE Trans. Magn.*, vol. 43, no. 10, pp. 3807–3815, Oct. 2007.

[15] Z. Kutchadze, A. Gheonjian, and R. Jobava, "Investigation of magnetic permeability of toroidal cores," in *Proc. 2019 Int. Symp. Electromagn. Compat. - EMC EUROPE*, 2019, pp. 498–503.

[16] V. Radonić, N. Blaz, and L. Zivanov, "Measurement of complex permeability using short coaxial line reflection method," *Acta Physica Polonica A*, vol. 117, pp. 820–824, 2010.

[17] M. Kacki, M. S. Rylko, J. G. Hayes, and C. R. Sullivan, "Measurement methods for high-frequency characterizations of permeability, permittivity, and core loss of Mn-Zn ferrite cores," *IEEE Trans. Power Electron.*, vol. 37, no. 12, pp. 15152–15162, Dec. 2022.

[18] A. M. Nicolson and G. F. Ross, "Measurement of the intrinsic properties of materials by time-domain techniques," *IEEE Trans. Instrum. Meas.*, vol. 19, no. 4, pp. 377–382, Nov. 1970.

[19] W. Weir, "Automatic measurement of complex dielectric constant and permeability at microwave frequencies," *Proc. IEEE*, vol. 62, no. 1, pp. 33–36, Jan. 1974.
[20] J. Baker-Jarvis, E. Vanzura, and W. Kissick, "Improved technique for determining complex permittivity with the transmission/reflection method," *IEEE Trans. Microw. Theory Techn.*, vol. 38, no. 8, pp. 1096–1103, Aug. 1990.
[21] K. Kikuchi, T. Kanie, and T. Takeo, "Measurement of the permeability in a ferrite core by superimposing bias current," *J. Int. Council Elect. Eng.*, vol. 4, no. 1, pp. 67–73, 2014.
[22] I. Schmidt and A. Enders, "Impedance measurements from 1–20 MHz with up to 200 A (50 Hz) bias-current for the optimization of high power high frequency coils," in *Proc. 2009 IEEE Int. Symp. Electromagn. Compat.*, 2009, pp. 147–150.
[23] M. Szewczyk, K. Kutorasinski, J. Pawłowski, W. Piasecki, and M. Florkowski, "Advanced modeling of magnetic cores for damping of high-frequency power system transients," *IEEE Trans. Power Del.*, vol. 31, no. 5, pp. 2431–2439, Oct. 2016.
[24] K. Kutorasiński, M. Szewczyk, M. Molas, and J. Pawłowski, "Measuring impedance frequency characteristics of magnetic rings with DC-bias current," *ISA Trans.*, vol. 143, pp. 723–739, 2023.
[25] J. Eberhardt, F. Caspers, and C. Vollinger, "Ferrite characterization for the design of an accelerating cavity with perpendicular biasing," *IEEE Trans. Nucl. Sci.*, vol. 63, no. 2, pp. 693–698, Apr. 2016.
[26] W. R. Smythe, "Reducing ferrite tuner power loss by bias field rotation," *IEEE Trans. Nucl. Sci.*, vol. 30, no. 4, pp. 2173–2175, Aug. 1983.
[27] C. Vollinger, F. Caspers, and E. Jensen, "The effect of 2-directional magnetic biasing used for tuning of a ferrite-loaded re-entrant cavity," *IEEE Trans. Nucl. Sci.*, vol. 60, no. 3, pp. 2170–2174, Jun. 2013.
[28] M. Harm, O. Kerfin, L. Oppermann, A. Enders, and T. Braunschweig, "Calibrated contactless impedance measurements with dc bias currents," in *Proc. 2018 Int. Symp. Electromagn. Compat. (EMC EUROPE)*, 2018, pp. 226–230.
[29] M. Harm, M. Rust, and O. Kerfin, "Evaluation of different techniques for contactless RF impedance measurements in dc power grids," in *Proc. 2020 Int. Symp. Electromagn. Compat. - EMC EUROPE*, 2020, pp. 1–6.
[30] B. Wunsch, S. Skibin, V. Forsstrom, and T. Christen, "Broadband modeling of magnetic components with saturation and hysteresis for circuit simulations of power converters," *IEEE Trans. Magn.*, vol. 54, no. 11, pp. 1–5, Nov. 2018.
[31] B. Wunsch, S. Skibin, T. Christen, and V. Forsstrom, "Improved EMC filter performance of ferrite cores based on hysteresis and saturation," in *Proc. 2019 Int. Symp. Electromagn. Compat. - EMC EUROPE*, 2019, pp. 444–449.
[32] X. Liu et al., "Behavioral modeling of complex magnetic permeability with high-order Debye model and equivalent circuits," *IEEE Trans. Electromagn. Compat.*, vol. 63, no. 3, pp. 730–738, Jun. 2021.
[33] S. Dobák, J. Füzer, P. Kollár, M. Strečková, R. Bureš, and M. Fáberová, "A comprehensive complex permeability approach to soft magnetic bulk cores from pure or resin coated Fe and pulverized alloys at elevated temperatures," *J. Alloys Compounds*, vol. 695, pp. 1998–2007, 2017.
[34] J. Muhlethaler, J. Biela, J. W. Kolar, and A. Ecklebe, "Core losses under the dc bias condition based on steinmetz parameters," *IEEE Trans. Power Electron.*, vol. 27, no. 2, pp. 953–963, Feb. 2012.
[35] Y. Ishikura, J. Imaoka, M. Noah, and M. Yamamoto, "Core loss evaluation in powder cores: A comparative comparison between electrical and calorimetric methods," in *Proc. 2018 Int. Power Electron. Conf. (IPEC-Niigata 2018-ECCE Asia)*, 2018, pp. 1087–1094.
[36] K. Nomura, S. Chizuwa, and T. Masuzawa, "High-frequency equivalent circuit of a ferrite common mode choke considering dc superimposition characteristics," in *Proc. 2024 IEEE Appl. Power Electron. Conf. Expo. (APEC)*, 2024, pp. 619–626.
[37] Chang Sung Corporation, "Magnetic powder cores." Accessed: Aug. 13, 2024. [Online]. Available: https://www.mhw-intl.com/assets/CSC/CSC_Catalog.pdf
[38] Micrometals, Inc., "Iron Powder Products Catalog." Accessed: Aug. 13, 2024. [Online]. Available: https://www.micrometals.com/design-and-applications/literature/
[39] D. M. Pozar, *Microwave Engineering*, 3rd ed.. Hoboken, NJ, USA: Wiley, 2005.
[40] L. D. Landau and E. M. Lifshitz, *Electrodynamics of Continuous Media*. New York, NY, USA: Pergamon, 1984.
[41] A. Schroeder, A. Savca, and T. Christen, "Dimensional resonances in magnetic powder cores," *Submitted to Proc. 2024 Int. Symp. Electromagn. Compat. - EMC EUROPE*, 2024.
[42] E. Limpert, W. A. Stahel, and M. Abbt, "Log-normal distributions across the sciences: Keys and clues," *BioScience*, vol. 51, no. 5, pp. 341–352, 2001.

Arne Schröder (Member, IEEE) received the Diploma and the Ph.D. degrees in electrical engineering from the Hamburg University of Technology, Hamburg, Germany, in 2009 and 2014, respectively.

Since 2020, he has been with Hitachi Energy Research, Baden-Dättwil, Switzerland. From 2014 to 2017, he was a Postdoctoral Researcher with the Institute of Applied Physics, University of Bern, Bern, Switzerland. In 2017, he joined ABB Corporate Research, Baden-Dättwil, Switzerland. His research interests include electromagnetic design and analysis of power electronic equipment as well as modeling of complex and multiscale systems.

Alexandru Savca received the BSc. degree, in 2022, in electrical engineering from the University of Twente, Enschede, The Netherlands, where he is currently working toward the M.Sc. degree in power electronics with an industrial graduation assignment with Hitachi Energy Research, Baden-Dättwil, Switzerland.

His research interests include battery technology, electromagnetic design and analysis, and thermal modeling of power electronic equipment.

Dierk Bormann received the Ph.D. degree in physics from the University of Heidelberg, Heidelberg, Germany, in 1992. Since 2020, he has been with Hitachi Energy Research in Västerås, Sweden.

After some years of academic research in the fields of statistical physics, superconductivity, and low-dimensional quantum systems, in 2000, he joined ABB Corporate Research, Västerås, Sweden, where his work focused mainly on transient and HF modeling of power apparatus and systems. He also supervised research students with the Royal Institute of Technology (KTH), Stockholm, Sweden, and Mälardalens University (MDU), Västerås, Sweden. His current research interests include the stability analysis and control of power electronic converters, transient dynamics and EMC in converter stations, as well as the mathematical modeling of electromagnetic and thermal material properties.